52nd IEEE Conference on Decision and Control
December 10-13, 2013. Florence, Italy

Wind Turbine Torque Control for Unsteady Wind Speeds Using Approximate-Angular-Acceleration Feedback

Jon Mullen and Jesse B. Hoagg
Department of Mechanical Engineering, University of Kentucky, Lexington, KY 40506-0503

***Abstract*— We present a wind turbine torque controller that incorporates approximate-angular-acceleration feedback. In contrast, the classical wind turbine torque controller generates a control signal that is proportional to the square of the turbine's angular velocity. We modify the classical torque controller by including an approximate-angular-acceleration term. This modified controller is shown numerically to capture more energy than the classical controller under unsteady (i.e., time-varying) wind speeds.**

I. Introduction

The finite supply and environmental impacts of fossil fuel necessitate sustainable methods of electric power production. One sustainable resource for power production is wind energy. A recent US Department of Energy study [1] proposes that wind account for twenty percent of US power production by 2030. Wind turbines are the predominant mechanism for capturing wind power. Moreover, horizontal-axis variable-speed wind turbines are the most common type of utility-scale turbine. Horizontal-axis variable-speed wind turbines generally operate in three regions; each of which is based on wind speed. See [2]–[5] for more details. In this paper, we focus on torque control for region 2.

A standard torque control method is given by $\tau_{\mathrm{g}}(t) = K_*\omega^2(t)$, where the optimal gain K_* depends on aerodynamic characteristics of the wind turbine [2], [3], [6]. This classical torque controller aims to drive the turbine's tip-speed ratio (i.e., the ratio of tip speed to wind speed) toward an optimal tip-speed ratio, which maximizes power capture. If the wind speed is constant and the optimal gain K_* is known, then the classical torque controller maximizes power capture (for a first-order wind-turbine model).

The classical torque controller does not address uncertainty in K_*, which can result from uncertainty in the turbine's aerodynamic properties. However, model uncertainty is addressed in [6]–[9].

While the classical torque controller maximizes power capture under constant wind speed, this controller does not generally maximize power capture under unsteady (i.e., time-varying) wind speed. Adaptive torque control is one approach to improve power capture with unsteady wind [10].

This paper presents a torque controller that incorporates approximate-angular-acceleration feedback. Specifically, we modify the classical torque controller by adding an approximate-angular-acceleration term. We show numerically that the approximate-angular-acceleration term helps to keep the turbine's tip-speed ratio near the optimal tip-speed ratio even if the wind speed is time varying. We analyze the stability properties of the torque controller with approximate-angular-acceleration feedback. Specifically, we show that under constant wind speed the modified controller yields a locally asymptotically stable closed-loop error system. Moreover, the modified torque controller is demonstrated on a first-order wind-turbine model under a variety of unsteady winds. This modified controller is shown to capture more energy than the classical controller. The modified torque controller is also implemented on the NREL/UpWind 5-MW baseline wind-turbine model [11] using NREL's FAST code.

II. Wind Turbine Model

Consider the first-order model of a horizontal-axis variable-speed wind turbine, which is given by

$$J\dot{\omega}(t) = \tau_{\mathrm{a}}(t) - \tau_{\mathrm{g}}(t), \tag{1}$$

where J is the rotor's moment of inertia, ω the rotor's angular velocity, τ_{a} the aerodynamic torque, and τ_{g} the generator torque, which is a nonnegative control. As the wind, which is traveling at speed $v(t)$, passes through the rotor's swept area, it follows that the available wind power is

$$P_{\mathrm{w}}(t) \triangleq \frac{1}{2}\rho\pi r^2 v^3(t), \tag{2}$$

where r is the rotor's radius and ρ is the density of air. The available wind power (2) cannot be transferred completely to the turbine because doing so would result in zero wind speed downstream of the turbine. In fact, the maximum power that can be transferred to the turbine is $C_{\mathrm{B}}P_{\mathrm{w}}$, where $C_{\mathrm{B}} = 16/27$ is the Betz limit [12]. The power transferred to the turbine is a function of the tip-speed ratio $\lambda(t) \triangleq \omega(t)r/v(t)$ and the pitch angle $\beta(t)$ of the turbine blades. Specifically, the power transferred to the turbine is

$$P_{\mathrm{a}}(t) \triangleq \mathcal{C}_{\mathrm{p}}(\lambda(t), \beta(t))P_{\mathrm{w}}(t), \tag{3}$$

where $\mathcal{C}_{\mathrm{p}} : (0, \infty) \times [\beta_{\min}, \beta_{\max}] \to (0, C_{\mathrm{B}})$ is the power coefficient, and $\beta_{\min}$ and $\beta_{\max}$ are the minimum and maximum blade pitch angles, respectively.

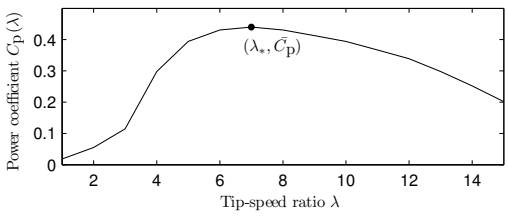

Fig. 1: The power coefficient $C_{\mathrm{p}}(\lambda)$ is a concave-down function of λ and has a unique maximum $\bar{C}_{\mathrm{p}}$ at $\lambda = \lambda_*$.

Next, let β_0 be the nominal blade pitch angle. For the purpose of developing the torque control, let $\beta(t) \equiv \beta_0$. Define $C_{\rm p}(\lambda) \triangleq \mathcal{C}_{\rm p}(\lambda, \beta_0)$, which is generally a concave-down function of λ as shown in Figure 1. It is assumed that $C_{\rm p}(\lambda)$ has a unique maximum, that is, there exists $\lambda_* \in (0,\ \infty)$, such that for all positive $\lambda \neq \lambda_*$, $C_{\rm p}(\lambda) < \bar{C}_{\rm p} \triangleq C_{\rm p}(\lambda_*)$. The maximizer λ_* is called the optimal tip-speed ratio. Furthermore, it is assumed that there exists a positive $\lambda_{\rm min} < \lambda_*$, such that for all $\lambda \in (\lambda_{\rm min}, \lambda_*)$,

$$\left(\frac{\lambda}{\lambda_*}\right)^3 < \frac{C_{\rm p}(\lambda)}{\bar{C}_{\rm p}}. \tag{4}$$

Assumption (4) is used in the stability analysis of the classical torque controller and is commonly invoked in the literature on wind turbine torque control [2], [3].

It follows from (2) and (3) that the power transferred to the turbine is $P_{\rm a}(t) = \rho\pi r^2 C_{\rm p}(\lambda(t))v^3(t)/2$, and, thus, the aerodynamic torque acting on the rotor is

$$\tau_{\rm a}(t) = \frac{P_{\rm a}(t)}{\omega(t)} = \frac{\rho\pi r^3 C_{\rm p}(\lambda(t))v^2(t)}{2\lambda(t)}. \tag{5}$$

Finally, combining (1) and (5) yields the turbine dynamics

$$J\dot{\omega}(t) = \frac{\rho\pi r^3 C_{\rm p}(\lambda(t))v^2(t)}{2\lambda(t)} - \tau_{\rm g}(t). \tag{6}$$

Wind turbines generally operate in three regions. In region 1, the wind speed $v(t)$ is less than the minimum wind speed $v_{\rm min}$ required to operate the turbine, and thus the rotor is kept stationary. In region 2, $v(t)$ is above $v_{\rm min}$ but below the turbine's rated wind speed $v_{\rm rated}$. The control objective in region 2 is to drive the tip-speed ratio $\lambda(t)$ to λ_*, which maximizes $P_{\rm a}(t)$. The primary control in region 2 is the generator torque $\tau_{\rm g}$. If $v(t) > v_{\rm rated}$, then the turbine is operating in region 3 and the optimal tip-speed ratio λ_* cannot be achieved because the rotor's angular velocity would exceed the rated value $\omega_{\rm rated} \triangleq v_{\rm rated}\lambda_*/r$. In region 3, the objective of regulating $\omega(t)$ to $\omega_{\rm rated}$ is achieved by adjusting the pitch angle β of the turbine blades.

III. Classical Torque Controller

Consider the torque controller of [2], [3], which is given by

$$\tau_{\rm g}(t) = K_*\omega^2(t), \tag{7}$$

where

$$K_* \triangleq \frac{\rho\pi r^5 \bar{C}_{\rm p}}{2\lambda_*^3}. \tag{8}$$

It is assumed that ρ, r, $\bar{C}_{\rm p}$, and λ_* are known, and $\omega(t)$ is measured. Adaptive versions of the classical torque controller are considered in [3], [9], [10] to address uncertainty in $\bar{C}_{\rm p}$ and λ_*. Combining (6)–(8) yields the closed-loop system

$$J\dot{\omega}(t) = \frac{\rho\pi r^3 C_{\rm p}(\lambda(t))v^2(t)}{2\lambda(t)} - \frac{\rho\pi r^5 \bar{C}_{\rm p}\omega^2(t)}{2\lambda_*^3}. \tag{9}$$

Substituting $\omega(t) = \lambda(t)v(t)/r$ into (9) and solving for $\dot{\lambda}(t)$ yields

$$\dot{\lambda}(t) = \frac{\rho\pi r^4\lambda^2(t)v(t)}{2J}\left[\frac{C_{\rm p}(\lambda(t))}{\lambda^3(t)} - \frac{\bar{C}_{\rm p}}{\lambda_*^3}\right] - \frac{\lambda(t)\dot{v}(t)}{v(t)}. \tag{10}$$

The following result states that, for a constant wind speed, the classical torque controller (7) and (8) drives $\lambda(t)$ to λ_*.

Proposition 1: Consider the closed-loop system (10), which consists of (6)–(8). Assume that $v(t) \equiv v_0$, where $v_0 < v_{\rm rated}$ is positive. Then, $\lambda(t) \equiv \lambda_*$ is a locally asymptotically stable equilibrium of (10). Furthermore, for all $\lambda(0) > \lambda_{\rm min}$, $\lim_{t\to\infty}\lambda(t) = \lambda_*$.

Proof: Define $e(t) \triangleq \lambda(t) - \lambda_*$ and $c_1 \triangleq \rho\pi r^4 v_0/(2J)$. Then (10), where $v(t) \equiv v_0$, can be written as

$$\dot{e}(t) = c_1(e(t)+\lambda_*)^2\left[\frac{C_{\rm p}(e(t)+\lambda_*)}{(e(t)+\lambda_*)^3} - \frac{\bar{C}_{\rm p}}{\lambda_*^3}\right]. \tag{11}$$

Consider the positive-definite, radially unbounded Lyapunov function $V(e) = e^2/2$. Evaluating the derivative of $V(e)$ along (11) yields $\dot{V}(e) = e\dot{e} = \gamma_1(e)\gamma_2(e)e$, where

$$\gamma_1(e) \triangleq \frac{c_1\bar{C}_{\rm p}}{(e+\lambda_*)},\ \ \gamma_2(e) \triangleq \frac{C_{\rm p}(e+\lambda_*)}{\bar{C}_{\rm p}} - \frac{(e+\lambda_*)^3}{\lambda_*^3}. \tag{12}$$

Next, define $e_{\rm min} \triangleq \lambda_{\rm min} - \lambda_*$ and $\mathcal{D} \triangleq \{e \in \mathbb{R} : e_{\rm min} < e < \infty\}$. For all $e > 0$, it follows from (12) that $\gamma_1(e) > 0$ and $\gamma_2(e) < 0$, which implies that $\dot{V}(e) < 0$. Next, for all $e \in (e_{\rm min}, 0)$, it follows from (4) and (12) that $\gamma_1(e) > 0$ and $\gamma_2(e) > 0$, which implies that $\dot{V}(e) < 0$. Therefore, for all $e \in \mathcal{D}\setminus\{0\}$, $V(e) > 0$ and $\dot{V}(e) < 0$, which implies that 0 is a locally asymptotically stable equilibrium of (11). Thus, λ_* is a locally asymptotically stable equilibrium of (10).

To show that for all $e(0) \in \mathcal{D}$, $\lim_{t\to\infty} e(t) = 0$, assume for contradiction that $V(e(t))$ does not converge to zero. Since $V(e(t))$ is decreasing and bounded from below by zero, it follows that there exists $\delta > 0$ such that for all $t \geq 0$, $V(e(t)) \geq \delta$. Now, consider two cases: (1) $e(0) \in (0, \infty)$ and (2) $e(0) \in (e_{\rm min}, 0)$. First, assume $e(0) \in (0, \infty)$. Since $V(e(t)) \geq \delta$ and $V(e(t))$ is decreasing, it follows that for all $t \geq 0$, $2\sqrt{\delta} \leq e(t) \leq e(0)$. Define $\psi_1 \triangleq \min_{2\sqrt{\delta}\leq e\leq e(0)} -\dot{V}(e)$, which is positive. Therefore, for all $t \geq 0$, $V(e(t)) - V(e(0)) = \int_0^t \dot{V}(e(\tau))d\tau \leq -\psi_1 t$, which implies that $V(e(t)) \leq V(e(0)) - \psi_1 t$. Thus, for all $t \geq V(e(0))/\psi_1$, $V(e(t)) < 0$, which is a contradiction.

Next, assume $e(0) \in (e_{\rm min}, 0)$. Thus, for all $t \geq 0$, $e(0) \leq e(t) \leq -2\sqrt{\delta}$. Define $\psi_2 \triangleq \min_{e(0)\leq e\leq -2\sqrt{\delta}} -\dot{V}(e)$, which is positive. Using the same argument as above, it follows that for all $t > V(e(0))/\psi_2$, $V(e(t)) < 0$, which is a contradiction. Therefore, $\lim_{t\to\infty} V(e(t)) = 0$, which implies that $\lim_{t\to\infty} e(t) = 0$. Thus, for all $\lambda(0) > \lambda_{\rm min}$, $\lim_{t\to\infty}\lambda(t) = \lambda_*$. □

Example 1: Constant wind speed. Consider the wind turbine (6), where $J = 388{,}500$ kg-m^2, $\rho = 1.12$ kg/m^3, $r = 21.5$ m, and $C_{\rm p}(\lambda)$ is given by Figure 1, where $\lambda_* = 7$ and $\bar{C}_{\rm p} = 0.44$. Let $v(t) \equiv 6$ m/s. The control objective is to drive $\lambda(t)$ to λ_*. Figure 2 shows the time histories of λ/λ_*, ω, and $\tau_{\rm g}$ with the classical torque controller (7) and

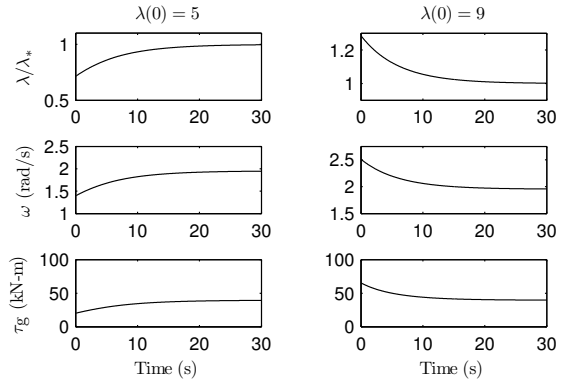

Fig. 2: Classical torque controller with constant wind speed. The classical torque controller (7) and (8) is implemented with the wind turbine (6), where $\lambda(0) = 5 < \lambda_*$ (left) and $\lambda(0) = 9 > \lambda_*$ (right). The tip-speed ratio $\lambda(t)$ converges to λ_*.

(8) connected in feedback, where $\lambda(0) = 5$ and $\lambda(0) = 9$. For each initial condition, the tip-speed ratio $\lambda(t)$ converges to λ_*, which agrees with the results of Proposition 1.

IV. Torque Controller with Approximate-Angular-Acceleration Feedback

The classical torque controller (7) and (8) drives the tip-speed ratio $\lambda(t)$ to the optimal tip-speed ratio λ_* under a constant wind speed. However, if the wind speed is time-varying, then the classical torque controller may not maximize energy capture. This section presents a new torque control strategy that incorporates approximate-angular-acceleration feedback, and is shown numerically to improve energy capture.

First, the new torque control strategy is motivated by demonstrating that the classical torque controller does not maximize energy capture if the wind speed is time-varying. It follows from (3) that the wind energy transferred to the turbine from t_0 to t_1 is

$$E_{\mathrm{a}}(t_1, t_0) \triangleq \int_{t_0}^{t_1} P_{\mathrm{a}}(\tau) d\tau = \frac{1}{2}\rho\pi r^2 \int_{t_0}^{t_1} C_{\mathrm{p}}(\lambda(\tau)) v^3(\tau) d\tau,$$

and this wind energy is either captured by the generator or transformed to kinetic energy. Thus, the energy captured by the generator is $E_{\mathrm{c}}(t_1, t_0) \triangleq E_{\mathrm{a}}(t_1, t_0) - \Delta E_{\mathrm{k}}(t_1, t_0)$, where $\Delta E_{\mathrm{k}}(t_1, t_0)$ is the rotor's change in kinetic energy.

Consider an example where the wind speed is time varying. Let $v_0 = v(t_0)$ and $\omega_0 = \omega(t_0)$. Next, assume that at t_0^+ the wind speed has a step change to v_1, that is, for all $t > t_0$, $v(t) = v_1$, and let $\omega_1 = \omega(t_1)$. In this case, $\Delta E_{\mathrm{k}}(t_1, t_0) = J(\omega_1^2 - \omega_0^2)/2$, which implies that $\Delta E_{\mathrm{k}}(t_1, t_0)$ is independent of the trajectory from ω_0 to ω_1. Thus, $E_{\mathrm{c}}(t_1, t_0) = (\rho\pi r^2 v_1^3/2) \int_{t_0}^{t_1} C_{\mathrm{p}}(\lambda(\tau)) d\tau - \Delta E_{\mathrm{k}}(t_1, t_0)$, which implies that $E_{\mathrm{c}}(t_1, t_0)$ is maximized by the trajectory from $\lambda(t_0)$ to $\lambda(t_1)$ that maximizes $\int_{t_0}^{t_1} C_{\mathrm{p}}(\lambda(\tau)) d\tau$. Next, let t_1 approach ∞ and assume $\lim_{t\to\infty} \lambda(t) = \lambda_*$, which implies that

$$E_{\mathrm{c}}(\infty, t_0) = \frac{\rho\pi r^2 v_1^3}{2} \int_{t_0}^{\infty} C_{\mathrm{p}}(\lambda(\tau)) d\tau - \frac{J(\lambda_*^2 v_1^2 - \lambda_0^2 v_0^2)}{2r^2}.$$

Thus, $E_{\mathrm{c}}(\infty, t_0)$ is maximized by maximizing $\int_{t_0}^{\infty} C_{\mathrm{p}}(\lambda(\tau)) d\tau$, and $C_{\mathrm{p}}(\lambda)$ is maximized by λ_*, which suggests that an effective control scheme is to make $\lambda(t) - \lambda_*$ small for all time.

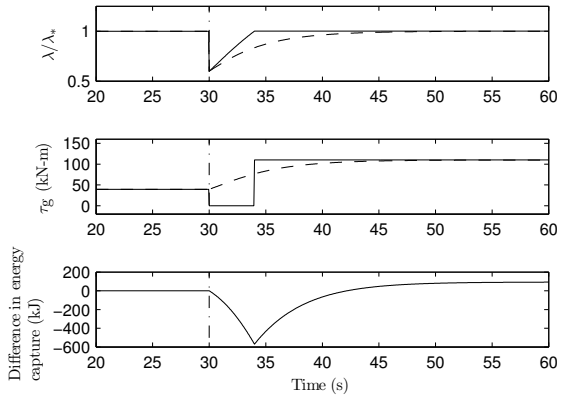

Fig. 3: The controller (13) (solid) captures more energy than the classical controller (dashed). The bottom plot shows the energy captured by the controller (13) minus the energy captured by the classical controller. In this example, the controller (13) captures 0.28% more energy from 30 s to 60 s than the classical controller.

Next, assume that $\lambda(t_0) = \lambda_*$ and $v_1 > v_0$, that is, the wind speed increases. In this case, $\lambda(t_0^+) < \lambda_*$, which means that $\lambda(t)$ must increase to reach λ_*. To allow $\lambda(t)$ to increase quickly, consider a torque control strategy that momentarily reduces the generator torque τ_{g} at t_0^+. Specifically, consider the torque control

$$\tau_{\mathrm{g}}(t) = \begin{cases} K_*\omega^2(t), & t \le t_0, \\ 0, & t_0 < t < t_0 + \Delta t, \\ K_*\omega^2(t), & t_0 + \Delta t < t, \end{cases} \tag{13}$$

where Δt is positive and K_* is given by (8).

Figure 3 compares the closed-loop response using the torque controller (13) to the response using the classical torque controller (7). In this example, $v_0 = 6$ m/s, $v_1 = 10$ m/s, $t_0 = 30$ s, $\lambda(t_0) = \lambda_* = 7$, and $\Delta t = 4$ s. Figure 3 shows that the controller (13) captures 0.28% more energy from 30 s to 60 s than the classical torque controller.

The controller (13) cannot be implemented in practice. First, $\tau_{\mathrm{g}}(t)$ is a function of wind speed $v(t)$, which is not assumed to be measured. Second, it could be difficult to determine the appropriate Δt. If Δt is too large, then $\lambda(t)$ will overshoot λ_*. Finally, the strategy (13) would not work if $v_1 < v_0$. In this case, it is better to momentarily increase the generator torque.

Since wind speed and wind acceleration are not assumed to be measured, this paper uses approximate angular acceleration of the turbine as a surrogate for wind acceleration. Consider the first-order linear filter

$$\dot{x}(t) = -px(t) - p\omega(t), \tag{14}$$

$$\alpha(t) = px(t) + p\omega(t), \tag{15}$$

where $p > 0$ and $x(0)$ is the initial condition. Note that the transfer function from ω to α is $ps/(s + p)$, which implies that for sufficiently large p, α approximates $\dot{\omega}$. Next, consider

the modified torque controller

$$\tau_{\rm g}(t) = \begin{cases} K_*\omega^2(t) - K_{\rm d}\alpha(t), & \alpha(t) < K_*\omega^2(t)/K_{\rm d}, \\ 0, & \alpha(t) \geq K_*\omega^2(t)/K_{\rm d}, \end{cases} \tag{16}$$

where K_* is given by (8), and $K_{\rm d} < J$ is nonnegative. Note that the controller (16) includes a saturation at zero to prevent the generator from supplying power to the turbine. Moreover, the modified torque controller (16) includes one term, which is identical to the classical torque control, and a second term, which provides approximate-angular-acceleration feedback.

Combining (6), (8), and (14)–(16), and substituting $\omega(t) = \lambda(t)v(t)/r$ yields the closed-loop system

$$\dot{\lambda}(t) = \begin{cases} \frac{\rho\pi r^4\lambda^2(t)v(t)}{2J}\left[\frac{C_{\rm p}(\lambda(t))}{\lambda^3(t)} - \frac{\bar{C}_{\rm p}}{\lambda_*^3}\right] \\ \quad + \frac{K_{\rm d}p[rx(t)+\lambda(t)v(t)]}{Jv(t)} - \frac{\lambda(t)\dot{v}(t)}{v(t)}, & \alpha(t) < \bar{\alpha}(\lambda(t)), \\ \frac{\rho\pi r^4 C_{\rm p}(\lambda(t))v(t)}{2J\lambda(t)} - \frac{\lambda(t)\dot{v}(t)}{v(t)}, & \alpha(t) \geq \bar{\alpha}(\lambda(t)), \end{cases} \tag{17}$$

$$\dot{x}(t) = -px(t) - p\lambda(t)v(t)/r, \tag{18}$$

where $\bar{\alpha}(\lambda(t)) \triangleq K_*\lambda^2(t)v^2(t)/(K_{\rm d}r^2)$.

The following result provides the stability properties of (17) and (18) under a constant wind speed.

Proposition 2: Consider the closed-loop system (17) and (18), which consists of (6), (8), and (14)–(16). Assume that $v(t) \equiv v_0$, where $v_0 < v_{\rm rated}$ is positive. Then, $(\lambda(t), x(t)) \equiv (\lambda_*, -\lambda_* v_0/r)$ is a locally asymptotically stable equilibrium of (17) and (18).

Proof: Define $\tilde{\lambda}(t) \triangleq \lambda(t) - \lambda_*$ and $\tilde{x}(t) = x(t) + \lambda_* v_0/r$. Let $c_1 \triangleq \rho\pi r^4 v_0/2J$. Since $v(t) \equiv v_0$, it follows from (17) and (18) that

$$\dot{\tilde{\lambda}}(t) = \begin{cases} f_1(\tilde{\lambda}(t), \tilde{x}(t)), & \alpha(t) < \bar{\alpha}(\tilde{\lambda}(t) + \lambda_*), \\ f_2(\tilde{\lambda}(t), \tilde{x}(t)), & \alpha(t) \geq \bar{\alpha}(\tilde{\lambda}(t) + \lambda_*), \end{cases} \tag{19}$$

$$\dot{\tilde{x}}(t) = f_3(\tilde{\lambda}(t), \tilde{x}(t)), \tag{20}$$

where

$$f_1(\tilde{\lambda}, \tilde{x}) \triangleq c_1(\tilde{\lambda} + \lambda_*)^2\left[\frac{C_{\rm p}(\tilde{\lambda} + \lambda_*)}{(\tilde{\lambda} + \lambda_*)^3} - \frac{\bar{C}_{\rm p}}{\lambda_*^3}\right] + \frac{K_{\rm d}p[r\tilde{x} + v_0\tilde{\lambda}]}{Jv_0},$$

$f_2(\tilde{\lambda}, \tilde{x}) \triangleq \frac{c_1 C_{\rm p}(\tilde{\lambda}+\lambda_*)}{(\tilde{\lambda}+\lambda_*)}$, and $f_3(\tilde{\lambda}, \tilde{x}) \triangleq -p\tilde{x} - pv_0\tilde{\lambda}/r$.

Next, consider the linearization about $(\tilde{\lambda}(t), \tilde{x}(t)) \equiv 0$. Note that $(\tilde{\lambda}(t), \tilde{x}(t)) \equiv 0$ implies that $\alpha(t) \equiv 0$, which is less than $\bar{\alpha}(0) > 0$. Thus,

$$A \triangleq \begin{bmatrix} \frac{\partial f_1}{\partial \tilde{\lambda}}(0,0) & \frac{\partial f_1}{\partial \tilde{x}}(0,0) \\ \frac{\partial f_3}{\partial \tilde{\lambda}}(0,0) & \frac{\partial f_3}{\partial \tilde{x}}(0,0) \end{bmatrix} = \begin{bmatrix} -c_2 + \frac{K_{\rm d}p}{J} & \frac{K_{\rm d}pr}{Jv_0} \\ -\frac{pv_0}{r} & -p \end{bmatrix},$$

where $c_2 \triangleq 3c_1\bar{C}_{\rm p}/\lambda_*^2 > 0$. The characteristic polynomial of A is $\mu_A(s) \triangleq s^2 + (c_2 + p\,(1 - K_{\rm d}/J))\,s + c_2 p$. Since $p > 0$ and $0 \leq K_{\rm d} < J$, it follows that the coefficients of $\mu_A(s)$ are positive, which implies that the roots of $\mu_A(s)$ are contained in the open-left-half complex plane. Thus $(\tilde{\lambda}(t), \tilde{x}(t)) \equiv 0$ is a locally asymptotically stable equilibrium of (19)–(20), which implies that $(\lambda(t), x(t)) \equiv (\lambda_*, -\lambda_* v_0/r)$ is a locally asymptotically stable equilibrium of (17) and (18). □

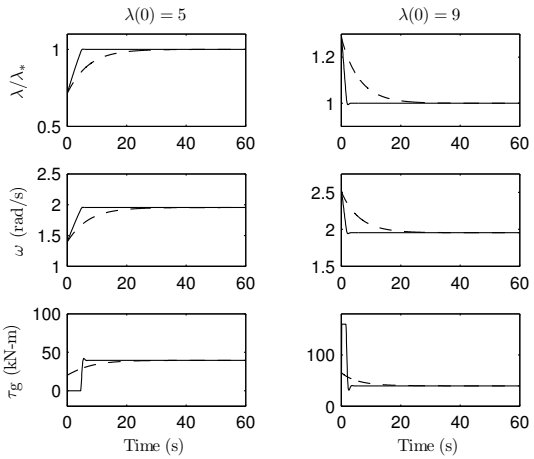

Fig. 4: Torque control with approximate-angular-acceleration feedback and constant wind speed. The modified torque controller (14)–(16) is implemented with the wind turbine (6) (solid), where $\lambda(0) = 5 < \lambda_*$ (left) and $\lambda(0) = 9 > \lambda_*$ (right). The results using the classical torque controller (7) (dashed) are shown for comparison. If the modified torque controller (14)–(16) is used, then $\lambda(t)$ converges to λ_* more quickly.

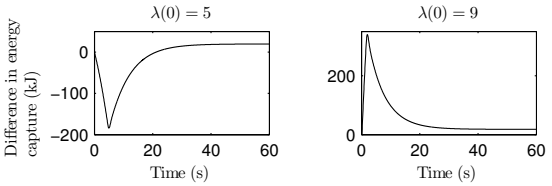

Fig. 5: The modified torque controller (14)–(16) and the classical torque controller (7) are each implemented with the wind turbine (6). The increase in energy capture by using the modified torque controller (14)–(16) is 19.7 kJ for the case where $\lambda(0) = 5$ (left), and 18.1 kJ for the case where $\lambda(0) = 9$ (right).

V. Numerical Simulations with 1st-Order Model

The following examples show that under time-varying wind conditions, the modified torque controller (14)–(16) can capture more energy than the classical torque controller (7).

Example 2: Constant wind speed. Consider the wind turbine model (6), where J, ρ, r, λ_*, and $C_{\rm p}(\lambda)$ are the same as in Example 1. The modified torque controller (14)–(16), with $p = 100$ and $K_{\rm d} = 369,075$, and the classical torque controller (7) are each connected in feedback with the wind turbine. Figure 4 shows the time histories of λ/λ_*, ω, and $\tau_{\rm g}$ for $\lambda(0) = 5$ and $\lambda(0) = 9$. The tip-speed ratio $\lambda(t)$ converges to λ_* in each case. The tip-speed ratio $\lambda(t)$ converges more quickly to λ_* if the modified torque controller (14)–(16) is used than if the classical torque controller (7) is used. Figure 5 shows the difference between the energy captured using the modified torque controller (14)–(16) and the classical torque controller (7). Over 60 seconds, more energy is captured by the modified torque controller (14)–(16).

Example 3: Sinusoidal wind speed. Consider the wind turbine model (6), where J, ρ, r, λ_*, and $C_{\rm p}(\lambda)$ are the same

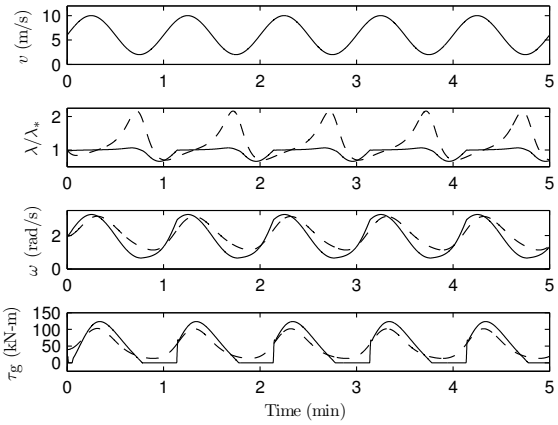

Fig. 6: Torque control with approximate-angular-acceleration feedback and sinusoidal wind speed. The modified torque controller (14)–(16) (solid) and the classical torque controller (7) (dashed) are each implemented with the wind turbine (6), where the wind speed is sinusoidal. If the modified torque controller (14)–(16) is used, then the tip-speed ratio $\lambda(t)$ is generally closer to λ_*.

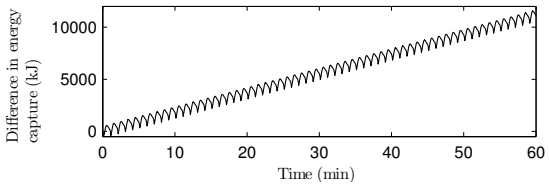

Fig. 7: The modified torque controller (14)–(16) and the classical torque controller (7) are each implemented with the wind turbine (6), where the wind speed is sinusoidal. Over the simulation time, the increase in energy capture by using the modified torque controller (14)–(16) is 11,100 kJ.

as in Example 1, and $\lambda(0) = \lambda_*$. Let $v(t) = 6+4\sin(\pi t/30)$ m/s. Figure 6 shows the time history of v, λ/λ_*, ω, and $\tau_{\rm g}$, with the modified torque controller (14)–(16) connected in feedback, with $p = 100$ and $K_{\rm d} = 369,075$. Figure 6 also shows the results with the classical torque controller (7) connected in feedback. The tip-speed ratio $\lambda(t)$ is generally closer to λ_* if the modified controller (14)–(16) is used than if the classical controller (7) is used. Figure 7 shows the difference between the energy captured by the modified torque controller (14)–(16) and the energy captured by the classical torque controller (7). More energy is captured by the modified torque controller (14)–(16).

Example 4: Stochastic wind speed. Consider the wind turbine model (6), where J, ρ, r, λ_*, and $C_{\rm p}(\lambda)$ are the same as in Example 1, and $\lambda(0) = \lambda_*$. Let $v(t) = 6 + a_2(t)$ m/s, where $a_2(t)$ is a zero-mean unit-variance Gaussian white noise realization passed through the four-pole filter $\omega_{\rm f}^4/(s+\omega_{\rm f})^4$, where $\omega_{\rm f} = 0.2\pi$ rad/s. Figure 8 shows the time history of λ/λ_*, ω, and $\tau_{\rm g}$, with the modified torque controller (14)–(16) connected in feedback, with $p = 100$ and $K_{\rm d} = 369,075$. Figure 8 also shows the results with the classical torque controller (7) connected in feedback. Figure 9 shows the difference between the energy captured by the modified torque controller (14)–(16) and the energy captured by the classical torque controller (7). More energy is captured

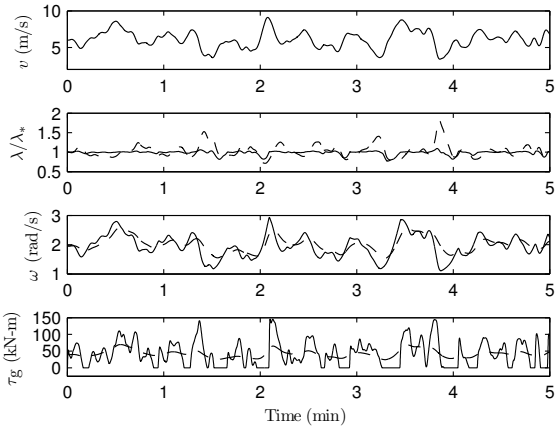

Fig. 8: Torque control with approximate-angular-acceleration feedback and stochastic wind speed. The modified torque controller (14)–(16) (solid) and the classical torque controller (7) (dashed) are each implemented with the wind turbine (6), where the wind speed is stochastic. If the modified torque controller (14)–(16) is used, then the tip-speed ratio $\lambda(t)$ is generally closer to λ_*.

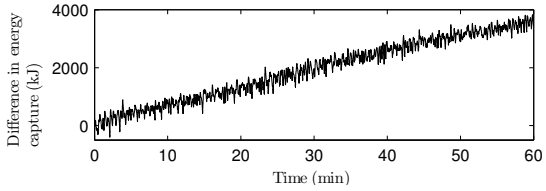

Fig. 9: The modified torque controller (14)–(16) and the classical torque controller (7) are each implemented with the wind turbine (6), where the wind speed is stochastic. Over the simulation time, the increase in energy capture by using the modified torque controller (14)–(16) is 3,470 kJ.

by the modified torque controller (14)–(16).

VI. Numerical Simulation with NREL's FAST Model

This section considers a wind turbine that is modeled using the National Renewable Energy Laboratory's FAST code [13]. The following simulations use the NREL/UpWind 5-MW baseline wind-turbine model [11], which is a three-blade, variable-speed wind turbine with rotor radius $r = 63$ m, rated wind speed $v_{\rm rated} = 11.4$ m/s, rated angular velocity $\omega_{\rm rated} = 1.27$ rad/s, and moment of inertia $J = 35,444,601$ kg-m^2. From [11], the classical torque controller gain is $K_* = 2,128,568$ kg-m^2. The optimal tip-speed ratio is $\lambda_* = 7.55$ and maximum power coefficient is $\bar{C_{\rm p}} = 0.482$.

The simulations show numerically that in a time-varying wind, the modified torque controller (14)–(16) can capture more energy than the classical torque controller (7).

Example 5: Sinusoidal wind speed. Consider the FAST wind turbine dynamics using the NREL/UpWind 5-MW model. Let $v(t) = 8 + 4\sin(\pi t/30)$ m/s, as shown at the top of Figure 10. The left side of Figure 10 shows the time histories of λ/λ_*, ω, and $\tau_{\rm g}$ with the classical torque controller (7), where $K_* = 2,128,568$. The right side of Figure 10 shows the same variables with the modified torque controller (14)–(16) connected in feedback, with $K_* = 2,128,568$, $p = 100$, and $K_{\rm d} = 2,425,000$. Figure 11 shows

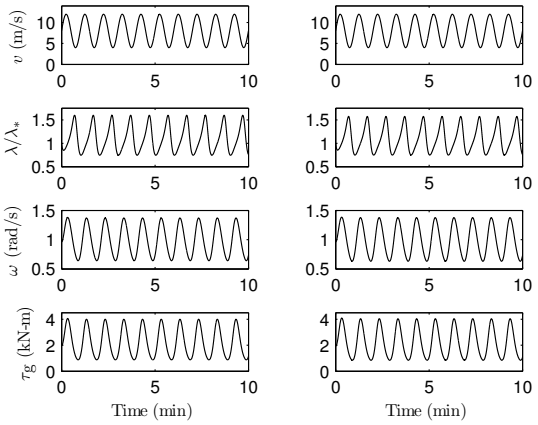

Fig. 10: Torque control with approximate-angular-acceleration feedback and sinusoidal wind speed. The classical torque controller (7) (left), and the modified torque controller (14)–(16) (right), are each implemented in feedback with the FAST wind turbine model, where the wind speed is sinusoidal.

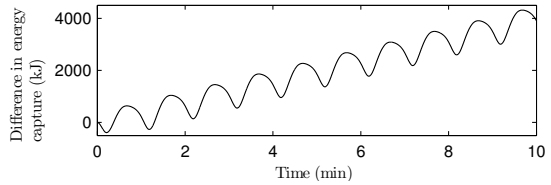

Fig. 11: The modified torque controller (14)–(16) and the classical torque controller (7) are each implemented with the 5-MW NREL/UpWind wind turbine using the FAST simulation where the wind speed is sinusoidal. Over the simulation time, the increase in energy capture by using the modified torque controller (14)–(16) is 3,900 kJ.

the difference between the energy captured by the modified torque controller (14)–(16) and the energy captured by the classical torque controller (7). More energy is captured by the modified torque controller (14)–(16).

Example 6: Stochastic wind speed. Consider the FAST wind turbine dynamics using the NREL/UpWind 5-MW model. Let $v(t) = 8 + a_2(t)$ m/s, where $a_2(t)$ is a zero-mean unit-variance Gaussian white noise realization passed through the four-pole filter $\omega_{\rm f}^4/(s+\omega_{\rm f})^4$, where $\omega_{\rm f} = 0.2\pi$ rad/s, as shown at the top of Figure 12. The left side of Figure 12 shows the time histories of λ/λ_*, ω, and $\tau_{\rm g}$ with the classical torque controller (7) connected in feedback, where $K_* = 2,128,568$. The right side of Figure 12 shows the same variables with the modified torque controller (14)–(16) connected in feedback, with $K_* = 2,128,568$, $p = 100$, and $K_{\rm d} = 2,425,000$. Figure 13 shows the difference between the energy captured by the modified torque controller (14)–(16) and the energy captured by the classical torque controller (7). More energy is captured by the modified torque controller (14)–(16).

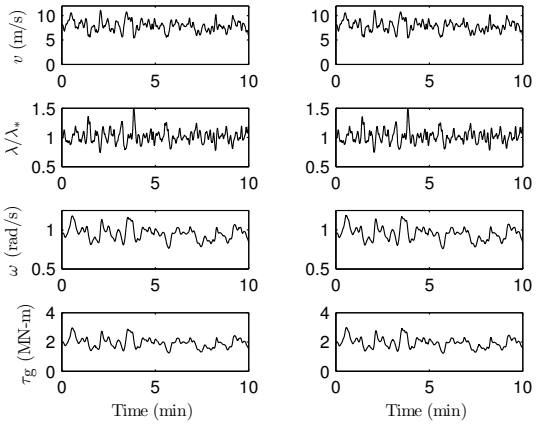

Fig. 12: Torque control with approximate-angular-acceleration feedback and stochastic wind speed. The classical torque controller (7) (left), and the modified torque controller (14)–(16) (right), are each implemented in feedback with the FAST wind turbine model, where the wind speed is stochastic.

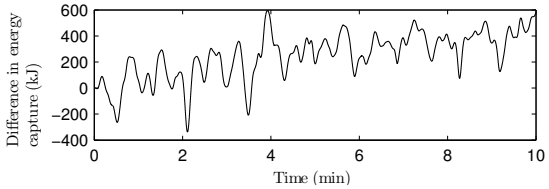

Fig. 13: The modified torque controller (14)–(16) and the classical torque controller (7) are each implemented with the 5-MW NREL/UpWind wind turbine using the FAST simulation where the wind speed is stochastic. Over the simulation time, the increase in energy capture by using the modified torque controller (14)–(16) is 576 kJ.

REFERENCES

[1] *20% Wind Energy by 2030: Increasing wind energy's contribution to U.S. electricity supply*. US Department of Energy, Report DOE/GO-102008-2567, 2008.

[2] L. Y. Pao and K. E. Johnson, "Control of wind turbines," *IEEE Control Syst. Mag.*, vol. 31, no. 2, pp. 44–62, 2011.

[3] K. E. Johnson, L. Y. Pao, M. J. Balas, and L. J. Fingersh, "Control of variable-speed wind turbines," *IEEE Control Syst. Mag.*, vol. 26, no. 3, pp. 70–81, 2006.

[4] J. Aho, A. Buckspan, J. Laks, P. Fleming, Y. Jeong, F. Dunne, M. Churchfield, L. Pao, and K. Johnson, "A tutorial of wind turbine control for supporting grid frequency through active power control," in *Proc. Amer. Contr. Conf.*, Montréal, Canada, 2012, pp. 3120–3131.

[5] P. Carlin, A. S. Laxson, and E. B. Mulhadi, "The history and state of the art of variable-speed wind turbine technology," *Wind Energy*, vol. 6, no. 2, pp. 129–159, 2003.

[6] F. Valenciaga and P. F. Puleston, "High-order sliding control for a wind energy conversion system based on a permanent magnet synchronous generator," *IEEE Trans. Energy Convers.*, vol. 23, no. 3, pp. 860–867, 2008.

[7] H. DeBattista and R. J. Mantz, "Dynamical variable structure controller for power regulation of wind energy conversion systems," *IEEE Trans. Energy Convers.*, vol. 19, no. 4, pp. 756–763, 2004.

[8] E. B. Muhando, T. Senjyu, H. Kinjo, and T. Funabashi, "Extending the modeling framework for wind generation systems: RLS-based paradigm for performance under high turbulence inflow," *IEEE Trans. Energy Convers.*, vol. 24, no. 1, pp. 211–221, 2009.

[9] K. E. Johnson, L. J. Fingersh, M. J. Balas, and L. Y. Pao, "Methods for increasing region 2 power capture on a variable speed wind turbine," *J. Solar Energy Eng.*, vol. 126, no. 4, pp. 1092–110, 2004.

[10] L. Díaz-Guerra, F. D. Adegas, J. Stoustrup, and M. Monros, "Adaptive control algorithm for improving power capture of wind turbines in turbulent winds," in *Proc. Amer. Contr. Conf.*, Montréal, Canada, 2012, pp. 5807–5812.

[11] J. Jonkman, S. Butterfield, W. Musial, and G. Scott, "Definition of a 5-MW reference wind turbine for offshore system development," National Renewable Energy Laboratory (NREL), Tech. Rep., 2009.

[12] T. Burton, *Wind Energy Handbook*. Wiley, 2001.

[13] J. Jonkman and M. Buhl, "FAST user's guide," National Renewable Energy Laboratory (NREL), Tech. Rep., 2005.